Modeling Domino Effects in Enzymes: Molecular Basis of the Substrate Specificity of the Bacterial Metallo-β-lactamases IMP-1 and IMP-6[†]

Peter Oelschlaeger,[‡] Rolf D. Schmid, and Juergen Pleiss*

Institute of Technical Biochemistry, University of Stuttgart, Allmandring 31, 70569 Stuttgart, Germany

Received February 4, 2003

ABSTRACT: Metallo-β-lactamases can hydrolyze a broad spectrum of β-lactam antibiotics and thus confer resistance to bacteria. For the *Pseudomonas aeruginosa* enzyme IMP-1, several variants have been reported. IMP-6 and IMP-1 differ by a single residue (glycine and serine at position 196, respectively), but have significantly different substrate spectra; while the catalytic efficiency toward the two cephalosporins cephalothin and cefotaxime is similar for both variants, IMP-1 is up to 10-fold more efficient than IMP-6 toward cephaloridine and ceftazidime. Interestingly, this biochemical effect is caused by a residue remote from the active site. The substrate-specific impact of residue 196 was studied by molecular dynamics simulations using a cationic dummy atom approach for the zinc ions. Substrates were docked in an intermediate structure near the transition state to the binding site of IMP-1 and IMP-6. At a simulation temperature of 100 K, most complexes were stable during 1 ns of simulation time. However, at higher temperatures, some complexes became unstable and the substrate changed to a nonactive conformation. To model stability, six molecular dynamics simulations at 100 K were carried out for all enzyme−substrate complexes. Stable structures were further heated to 200 and 300 K. By counting stable structures, we derived a stability ranking score which correlated with experimentally determined catalytic efficiency. The use of a stability score as an indicator of catalytic efficiency of metalloenzymes is novel, and the study of substrates in a near-transition state intermediate structure is superior to the modeling of Michaelis complexes. The remote effect of residue 196 can be described by a domino effect: upon replacement of serine with glycine, a hole is created and a stabilizing interaction between Ser196 and Lys33 disappears, rendering the neighboring residues more flexible; this increased flexibility is then transferred to the active site.

Metallo-β-lactamases have recently raised a major concern because of their capability to hydrolyze a broad spectrum of β-lactam antibiotics and thus confer resistance to bacteria (*1*−*3*). β-Lactam compounds are the most widely used antimicrobial agents applied for the treatment of infectious diseases. Together with serine-β-lactamases [classes A, C, and D (*4*)] that use a serine-dependent mechanism, metallo-β-lactamases (class B) form the enzyme group of β-lactamases (EC 3.5.2.6). Metallo-β-lactamases use zinc ions to activate a hydroxide ion, the nucleophilic agent attacking the amide bond of the β-lactam ring (*5*, *6*). After hydrolysis, β-lactams are inactivated and can no longer exert their antibiotic function, the inhibition of a transpeptidase involved in cell wall biosynthesis (*7*, *8*). Many β-lactams, especially second-, third-, and fourth-generation cephalosporins, have been designed that cannot be hydrolyzed by certain β-lactamases and thus are active against many nosocomial strains (*9*). However, the rapid evolution of bacterial β-lactamases, mainly due to the short generation time of bacteria and enhanced selective pressure imposed by application of antibiotics, continues to generate new enzyme variants. Protein evolution has been investigated in detail for the serine-β-lactamases, which has resulted in extended spectrum β-lactamases (ESBL),[1] mainly variants of the TEM and SHV enzymes (*10*, *11*).

Although metallo-β-lactamase activity was observed long ago (*12*), minor attention was paid to it as a clinical problem until the past decade (*13*). The first crystal structure to be resolved was that of the mononuclear *Bacillus cereus* enzyme BcII (*14*). It revealed a new protein fold ($\alpha\beta\beta\alpha$), now known as the metallo-β-lactamase fold (*15*). In the years that followed, three structures of binuclear metallo-β-lactamases of bacterial origin were determined: CcrA from *Bacteroides fragilis* (*16*), L1 from *Stenotrophomonas maltophilia* (*17*), and the imipenemase IMP-1 from *Pseudomonas aeruginosa* (*18*). Although with lower affinity, BcII can also bind a second zinc ion, and it has been considered an intermediate between mono- and binuclear metallo-β-lactmases (*19*). It has been shown that in CcrA, the second zinc ion stabilizes a substrate intermediate after hydrolysis of the β-lactam ring (*5*) and thus increases k_{cat} by a factor of 375 and k_{cat}/K_M by a factor of ∼10 compared to the values of a genetically

[†] This work was supported by the German Federal Ministry of Education and Research (Project PTJ 31/0312702).

* To whom correspondence should be addressed. E-mail: itbjpl@po.uni-stuttgart.de. Fax: (+49) 711-685-3196. Telephone: (+49) 711-685-3191.

[‡] Present address: Mayo Group, Division of Biology, Mail Code 114−96, California Institute of Technology, Pasadena, CA 91125.

[1] Abbreviations: AMP, ampicillin; CAZ, ceftazidime; CEF, cephalothin; CTX, cefotaxime; ESBL, extended spectrum β-lactamase(s); IMP, imipenem; IMP-n, imipenemase n; LOR, cephaloridine; MD, molecular dynamics; PEN, benzylpenicillin; rmsd, root-mean-square deviation(s).

10.1021/bi0300332 CCC: $25.00
Published on Web 07/08/2003

engineered mononuclear variant (*20*). These observations indicate that a second zinc ion might be an evolutionary adaptation toward more efficient β-lactam hydrolysis. IMP-1 very efficiently hydrolyzes a broad spectrum of substrates, including penicillins, cephalosporins, and carbapenems (*21*). Therefore, it has been denoted as an ESBL (*22*). The fact that some metallo-β-lactamases can efficiently hydrolyze carbapenems makes them even more dangerous than ESBL with a serine-dependent mechanism, which cannot inactivate these antibiotics.

Several variants of the *P. aeruginosa* enzyme IMP-1, isolated from different genera, have been reported (*2*, *3*, *21*, *23*−*28*). IMP-6 and IMP-3 are closely related to IMP-1: IMP-6 differs from IMP-1 in only one amino acid and IMP-3 in two. The substrate spectra of these enzymes were systematically investigated (*21*). Determination of k_{cat}/K_M values for the hydrolysis of different β-lactam compounds with purified enzymes indicated similar substrate spectra for IMP-6 and IMP-3, but a significantly different and extended substrate spectrum for IMP-1. It was demonstrated that the Gly196Ser mutation is responsible for this observation. This amino acid is not catalytically active but adjacent to the zinc ligand His197. In the structurally similar BcII and CcrA enzymes, the corresponding amino acid is also a glycine; in the structurally different L1 enzyme, it is a proline. Although the Gly196Ser mutation had no significant effect on k_{cat}/K_M values toward cephalothin and cefotaxime, two cephalosporins with an acetoxy group at the dihydrothiazine ring (R_2), it led to increases in k_{cat}/K_M by factors of 7 and 10 toward cephaloridine and ceftazidime, respectively, two cephalosporins with a pyridinium moiety at the respective position. For imipenem, benzylpenicillin, and ampicillin, it even resulted in 40-fold higher k_{cat}/K_M values. These results led Iyobe *et al*. to the conclusion that the Gly → Ser mutation resulted from selective pressure (*21*). To date, the dramatic effect of replacing the side chain at position 196 could not be explained at a molecular level, particularly because this residue neither is involved in zinc coordination nor is in direct contact with the substrate. In contrast to mutations in the binding site which have an immediate and localized effect on the interaction between the binding sites of various enzymes and their substrates (*10*, *11*, *29*), the side chain at position 196 acts at a distance.

Molecular modeling is a powerful tool for obtaining insight into the mechanism of metallo-β-lactamases. Molecular dynamics (MD) simulations and combinations of quantum chemical and molecular mechanical calculations indicated that in the mononuclear *B. cereus* enzyme BcII, a hydroxide rather than a water molecule is the nucleophilic agent coordinated to the zinc ion (*6*). In the binuclear CcrA from *Ba. fragilis*, the hydroxide functions as a bridging ligand between the two zinc ions and, in agreement with structural data (*16*), is responsible for the small Zn1−Zn2 distance of 3.5 Å (*30*). In contrast, when this bridge breaks down, an event which is favored if the active site Asp103 is protonated, the Zn1−Zn2 distance increases to 4.5−5 Å (*30*). Using MD simulations and a cationic dummy atom approach for the zinc ions, which has been shown to be practical for mononuclear (*31*) and binuclear zinc centers (*32*), a similar Zn1−Zn2 distance was observed in IMP-1, when an intermediate structure of the cephalosporin substrate (CEF) was docked (*54*). This intermediate occurs immediately before protonation of the substrate, which is the rate-limiting step in the catalytic cycle, and lacks the bridging hydroxide (*5*).

In particular, molecular modeling has identified structural determinants of substrate binding, as there are no crystal structures of enzyme−substrate complexes available. Thus, Michaelis complexes of L1 in complex with AMP, CAZ, and IMP (*17*), BcII with PEN (*33*), IMP-1 with IMP (*34*), and CcrA with IMP (*35*) were modeled. In the latter study, it was concluded that a Michaelis complex with the intact Zn1−OH−Zn2 bridge (Zn1−Zn2 distance of 3.5 Å) could be followed by an intermediate, in which the bridge is broken (Zn1−Zn2 distance of 4.4 Å), and the hydroxide is only bound to Zn1. In this structure, the substrate was bound more tightly and the hydroxide is more nucleophilic, both favoring the attack of the amide bond. Consequently, this structure was interpreted as an intermediate preceding the catalytic event. A complex of an enzyme and a substrate that exhibited good conversion in experiment [IMP-1−CEF, $k_{cat}/K_M = 32.5$ s^{-1} μM^{-1} (*21*)] could be modeled at 300 K and remained stable for more than 1 ns (*54*). In this model, the substrate interacted noncovalently with the zinc ions, which were represented by a cationic dummy atom approach (*31*, *32*). The geometry of the active site equilibrated within the first 200 ps and then remained stable until 1.2 ns of simulation. The Zn1−Zn2 distance increased to 4.6 Å, 1 Å more than in the inhibitor-bound structure in which the inhibitor thiolate sulfur acts as a bridging ligand (*18*). Ligand−zinc distances were between 1.9 and 2.2 Å, and all ligand−zinc−ligand angles were in the range of 99−118°, indicating a stable tetrahedral coordination of the zinc ions. According to Suarez *et al*. (*35*), the Zn1−Zn2 distance would increase before the nucleophilic attack occurs. Modeling of the two Michaelis complexes (*35*) and the intermediate complex (*54*) confirms the proposed catalytic mechanism (*5*) and indicates that the Zn1−Zn2 distance changes by ∼1 Å in the catalytic cycle.

The aim of this paper is to investigate the molecular basis of substrate specificity of binuclear metallo-β-lactamases. In experiments with IMP-1 and IMP-6 (*21*), it has been shown that there are two types of substrates: CEF and CTX are converted well and are insensitive to the Gly196Ser mutation, while LOR, CAZ, AMP, PEN, and IMP are poorly converted and sensitive to the mutation. We employed MD simulations in an effort to understand why different substrates result in different k_{cat}/K_M values, and how changes in the sequence and structure of the enzyme change k_{cat}/K_M values for the mutation-sensitive substrates, whereas they do not for mutation-insensitive substrates. As representatives for the mutation-sensitive substrates, two cephalosporins, LOR and CAZ, were selected to exclude influences of the substrate core and facilitate comparison to the mutation-insensitive cephalosporins (CEF and CTX). Thus, eight combinations of IMP-1 and IMP-6 in complex with four different substrates were investigated.

COMPUTATIONAL METHODS

Preparation of the Protein−Substrate Complex. The coordinates of molecule A in PDB entry 1DD6 (*18*) were used to model IMP-1. If not mentioned otherwise, titratable groups were treated as suggested by the program *protonate* of the *AMBER 6.0* software package (*36*) at pH 7.0. The

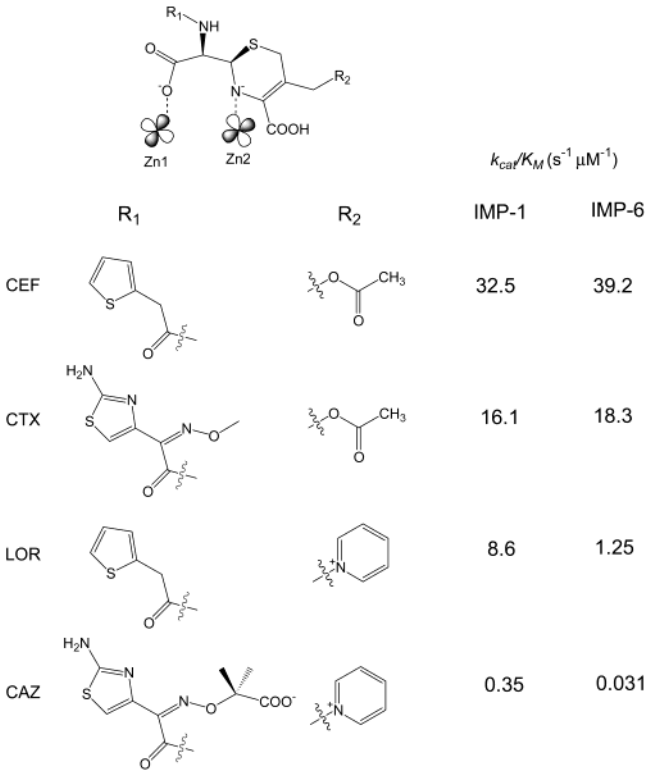

FIGURE 1: Binding mode of the anionic cephalosporin intermediates. The cationic dummy atoms arranged tetrahedrally around the zinc center are displayed. For clarity, the amino acid ligands oriented toward the other dummy atoms are not displayed. Side chains R_1 and R_2 are specified for cephalothin (CEF), cefotaxime (CTX), cephaloridine (LOR), and ceftazidime (CAZ). At the right, the k_{cat}/K_M values from experiment (*21*) are supplied.

zinc ions in the active site were modeled using the cationic dummy atom approach (*31*). This procedure also includes the deprotonation of titratable groups in the first coordination sphere of zinc ions and protonation of the second coordination sphere. In the first coordination sphere, Asp81, Cys158, and the carboxyl group resulting from hydrolysis of the amide bond in the cephalosporins were deprotonated. On the basis of *ab initio* calculations, it has been shown that the proton dissociation energy of imidazole when coordinated to Zn^{2+} is dramatically reduced, suggesting the existence of imidazolate as a zinc ligand in proteins (*37*). There is also experimental evidence for zinc-bound histidinate in proteins (*38*, *39*). Therefore, His77, His79, His139, and His197 were treated as histidinates. Partial charges of histidinate were taken from Pang *et al*. (*31*). In the second coordination sphere, the carboxyl group at the six-membered dihydrothiazine ring of the β-lactam substrates and Asp170 were protonated. The latter can be interpreted as an acceptor for the proton from the zinc-coordinating His79, and it has been shown that such a protonation state is energetically favored (*37*). The β-lactam substrates (Figure 1) were built using the *MolBuilder* module of the *InsightII* program (Accelrys, San Diego, CA) and minimized semiempirically with the *AMPAC/MOPAC* module of *InsightII*. Partial charges were fitted using the *RESP* program of *AMBER 6.0* to reproduce the *ab initio* HF/6-31G* electrostatic potential calculated by *Gaussian 98* (Gaussian, Pittsburgh, PA). The parm96 version of the all-atom *AMBER* force field (*40*) was used to represent the protein system. Parameters for the substrates were defined according to similar structures in the *AMBER* libraries. After removal of the inhibitor, the hydrolyzed CEF was manually docked into the active site guided by the structure of the inhibitor. The anionic nitrogen resulting from the hydrolyzed amide bond was coordinated to Zn2 and one oxygen of the carboxylate to Zn1 (Figure 1). The partial charges of the anionic nitrogen were as follows: -0.4984 in CEF, -0.4473 in CTX, -0.4709 in LOR, and -0.3341 in CAZ. The partial charges of the carboxylate oxygens were as follows: -0.8016 in CEF, -0.8160 in CTX, -0.7660 in LOR, and -0.7691 in CAZ. The 2-thiophenyl-1-acetyl amino residue (R_1) of CEF was oriented according to the 2-phenyl-1-ethyl residue of the inhibitor and the acetoxy group (R_2) according to the (5-methylene-1-tetrazole)-2-thiophenyl residue of the inhibitor as reported previously (*54*). Complexes of the other cephalosporins were generated starting from the IMP-1−CEF complex. The hydrolyzed desacetoxy-7-aminocephalosporanic acid was kept completely fixed, and the side chains were oriented according to CEF. To generate LOR, the acetoxy group of CEF in R_2 was replaced with pyridinium. R_1 of CTX and ceftazidime CAZ were built starting from CEF and CTX, respectively. The oxime moieties in R_1 were oriented toward the surface of the protein. The coordinate files of IMP-6 in complex with the four cephalosporins were generated from the IMP-1 complexes by exchanging Ser196 with glycine.

Using the *xLEaP* program of the *AMBER 6.0* software package, all structures were solvated in a truncated octahedron of TIP3P water with a minimal distance of 10.0 Å between the box boundary and the protein and neutralized with Na^+ ions.

MD Simulations and Stability Ranking. Minimizations and MD simulations were performed using the *Sander* program of the *AMBER 6.0* software package. The resulting systems of ~25000 atoms were energy minimized for 1000 steps (500 steepest descent and 500 conjugate gradient) and heated by MD simulation to 100 K starting at 10 K. The time step was 1 fs, and the *SHAKE* algorithm (*41*) was applied to all bonds containing hydrogen atoms. Six simulations of each enzyme−substrate combination were performed with different initial velocity distributions. During the heating process from 10 to 100 K, the positions of the zinc ions and the substrate were constrained to maintain a Zn1−Zn2 distance of ~3.6 Å. After the temperature of 100 K was reached, the constraints were gradually decreased, and the systems were allowed to equilibrate during an unconstrained MD simulation for 200 ps. The resulting zinc coordination was examined, and complexes were identified as stable (initial zinc coordination maintained) or unstable. A maximum number of three stable complexes were selected and heated to 200 K, equilibrated, simulated for 200 ps, and again examined with respect to stability. Those that had remained stable were heated to 300 K, equilibrated, simulated for 200 ps, and again examined for stability. For each simulation that was stable at a certain temperature, a score of 1 was assigned to the corresponding enzyme−substrate combination. At 100 K, a maximum score of 3 could be assigned for those complexes selected for further heating. Thus, a stability ranking was obtained ranging from a score of 0 (none of the simulations at 100 K of a certain enzyme−substrate combination yielded a stable structure) to 9 (at least three stable structures were obtained after the simulations at 100 K, and all of these

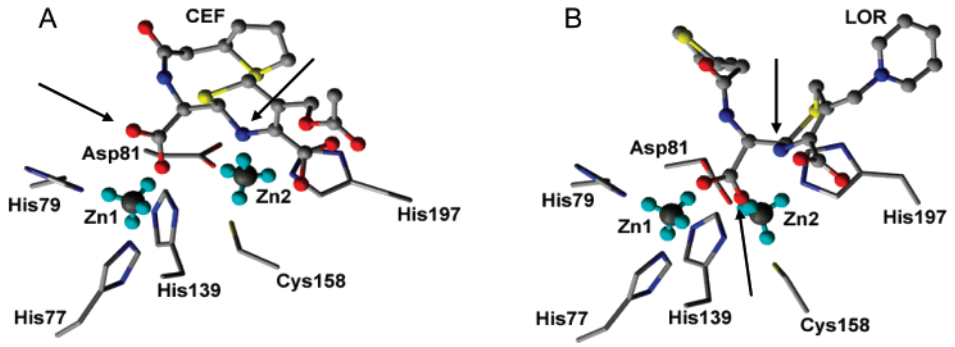

FIGURE 2: (A) Average structure of the IMP-1−CEF complex in the intact intermediate structure after unconstrained MD simulation at 300 K. (B) Average structure of the IMP-6−LOR complex after breakdown of the intermediate structure. Atoms are colored as follows: gray for C, red for O, blue for N, yellow for S, dark gray for zinc, and cyan for dummy atom. The amino acids are displayed as sticks and the substrates and the zincs as balls and sticks. Amino acids are labeled according to the system for PDB entry 1DD6 (*18*) at Cα. Substrates are labeled at R_1. Arrows indicate the anionic nitrogen of the substrate intermediate and the carboxylate oxygen that does not coordinate to zincs in stable complexes but replaces the nitrogen in unstable complexes.

remained stable at 200 and 300 K). The resulting scores were plotted against experimentally determined k_{cat}/K_M values (*21*).

Geometrical Examination of the Active Site. To examine the geometry of the active site, average structures over the last 10 ps of each simulation were generated using the *ptraj* program of the *AMBER 6.0* software package. Visual inspection of the trajectories was done with the *VMD* software (*42*). The distance between the substrate and Zn2 as well as the angle α between Zn2, the adjacent dummy atom, and the substrate anionic nitrogen and the angle between Zn2, the dummy atom, and the oxygen of the carboxylate resulting from substrate hydrolysis were tracked over the course of the simulations using *ptraj*. In structures which were stable at 100 K, α was measured over the last 10 ps of the 200 ps simulations and averaged. For each enzyme−substrate combination, the average of α in each simulation was calculated and plotted against the experimentally determined k_{cat}/K_M value (*21*).

To investigate the influence of R_2, distances from the ester oxygens (CEF and CTX) or the pyridinium nitrogen (LOR and CAZ) to surrounding residues were measured in average structures generated from the last 10 ps of the 200 ps simulations at 100 K of stable structures. Likewise, the distances between the side chain oxygen of Ser196 and the side chain nitrogen of Lys33 and between His197 Nδ and the Pro32 carbonyl oxygen were measured. The resulting average distances for each enzyme−substrate complex were compared to the k_{cat}/K_M values obtained in experiment (*21*). Average structures were superposed using *Swiss PDB Viewer* (Glaxo Smith Kline, Geneva, Switzerland). To determine the flexibility of the His197 side chain, rmsd of the heavy atoms from the average structures were monitored over the course of simulations using *ptraj*.

RESULTS

Dependence of the Stability of Modeled Structures on Enzyme−Substrate Combination and Simulation Temperature. Eight metallo-β-lactamase−cephalosporin complexes were modeled by MD simulation to identify geometrical parameters which correlate with the experimentally determined k_{cat}/K_M values (*21*). An intermediate structure before the rate-limiting step in catalysis (*5*) was chosen. Three 200 ps simulations of IMP-1 in complex with CEF (k_{cat}/K_M = 32.5 s^{-1} μM^{-1}) with different initial velocities were performed at 300 K. The complex remained stable in all simulations, and all zinc−ligand distances were within 1.9 and 2.2 Å (Figure 2A). Ligand−zinc−ligand angles were close to the optimal tetrahedral angle (96−121°). The Zn1−Zn2 distance varied (4.4−5.7 Å) but was always significantly larger than in the inhibitor-bound crystal structure (3.6 Å). The overall structures resulting from different initial velocities varied (e.g., in the orientation of the loop region, data not shown). However, in all simulations, the zinc coordination and the intermediate structure of the substrate remained stable. Multiple simulations of the IMP-6−CEF complex (k_{cat}/K_M = 39.2 s^{-1} μM^{-1}) gave consistent results.

In contrast, when both proteins were simulated in complex with LOR (k_{cat}/K_M = 8.6 s^{-1} μM^{-1} for IMP-1 and 1.25 s^{-1} μM^{-1} for IMP-6) with different initial velocities, the intermediate structures always broke down within the first 100 ps at 300 K or even during the heating of the systems. In all cases, the breakdown was due to the anionic nitrogen of the β-lactam intermediate losing contact with Zn2. A typical structure after the intermediate breakdown for the IMP-6−LOR complex is shown in Figure 2B. The substrate nitrogen was replaced with an oxygen atom of the carboxyl group resulting from amide bond hydrolysis of the substrate. Such a replacement is tracked by analysis of the distances between Zn2 and the anionic nitrogen, the leaving ligand, and the carboxylate oxygen, the entering ligand, as well as the angle between Zn2, the connecting dummy atom, and the leaving or entering ligand (Figure 3). The replacement occurred at the very beginning of the simulation within less than 1 ps. The carboxylate oxygen flipped instantaneously into a nearly tetrahedral coordination to Zn2 (Zn2−COO distance of 1.93 Å, Zn2−dummy atom−COO angle of 172°). The anionic substrate nitrogen moved away from Zn2 during the first 75 ps and then remained at a constant distance of 5.5 Å. In addition, the pyridinium moiety moved out of its original position and eventually pressed toward the Trp28 side chain in the loop covering the active site. A reconstitution of the original intermediate structure was never observed. The partial charge of the carboxylate oxygen was more negative than that of the anionic nitrogen (see Computational Methods). Consequently, the oxygen was bound more tightly to Zn2 than the anionic nitrogen before the replacement at distances of 1.93 and 2.16 Å, respectively.

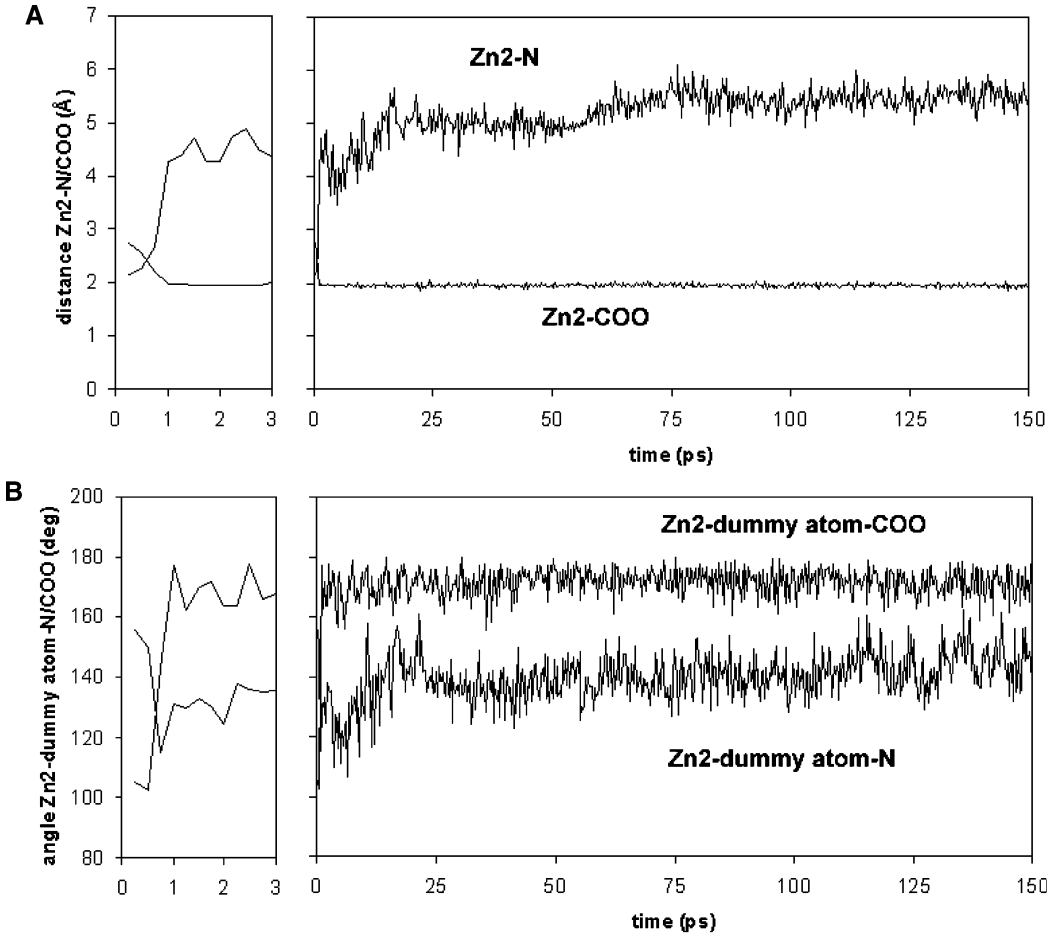

FIGURE 3: (A) Zn2−anionic substrate nitrogen and Zn2−substrate carboxylate oxygen distances over the course of an unconstrained MD simulation of the IMP-6−LOR complex at 300 K. (B) α (Zn2−dummy atom−anionic substrate nitrogen) and Zn2−dummy atom−substrate carboxylate oxygen angles tracked over the course of the simulation. The windows at the left indicate the time course of the initial 3 ps.

To investigate whether sensitive enzyme−substrate complexes would be stable at a lower temperature, they were simulated at 100 K without constraints. In the majority of simulations, they remained stable, even when simulations were carried out for 1 ns. As in the simulations of the IMP-1−CEN complex at 300 K, the zinc−ligand distances were between 1.9 and 2.2 Å and the ligand−zinc−ligand angles were close to the tetrahedral angle in stable simulations. The Zn1−Zn2 distances varied from 4.1 to 5.8 Å. This empirical approach shows that enzyme−substrate complexes with higher k_{cat}/K_M values are more likely to remain stable in MD simulations than complexes with lower k_{cat}/K_M values, and that complexes are more stable at lower temperatures than at higher temperatures. This sensitivity of the system was used to develop a method for ranking of enzyme−substrate complexes by their stability.

Stability Ranking by Progressive Heating. The following procedure was established to obtain a stability ranking of eight complexes of the two metallo-β-lactamases IMP-1 and IMP-6 with four cephalosporin substrates (CEF, CTX, LOR, and CAZ). After minimization, the complexes were heated to 100 K and simulated for 200 ps. This was done six times for each complex with different initial velocities. Under these conditions, at least one simulation for each enzyme−substrate combination led to a stable complex. Unstable structures were discarded. From the stable structures, at most three per complex were randomly selected, heated to 200 K, and simulated. Again, unstable structures were discarded, and stable structures were further heated to 300 K and simulated. From the results that were obtained, a stability ranking was deduced by counting stable structures at the three temperatures, thus allowing a maximum score of 9 (Table 1). For combinations with k_{cat}/K_M values of >30 s^{-1} μM^{-1} (IMP-1−CEF and IMP-6−CEF), all simulations were stable at all temperatures. For combinations with k_{cat}/K_M values between 20 and 10 s^{-1} μM^{-1} (IMP-1−CTX and IMP-6−CTX), one breakdown at 300 K was observed, while all simulations at lower temperatures were stable. For combinations with k_{cat}/K_M values between 10 and 1 s^{-1} μM^{-1} (IMP-1−LOR and IMP-6−LOR), in 10 of 12 simulations at 100 K, the intermediate structure was stable, whereas only 50% remained stable at 200 K. Of these three complexes, only one remained stable at 300 K. Only 25% of the complexes with k_{cat}/K_M values of <1 s^{-1} μM^{-1} (IMP-1−CAZ and IMP-6−CAZ) were stable at 100 K. Of these three complexes, one was stable at 200 K and none at 300 K. Thus, for all enzyme−substrate combinations with low k_{cat}/K_M values (IMP-1−LOR, IMP-6−LOR, IMP-1−CAZ, and IMP-6−CAZ), the number of stable simulations decreased significantly with increasing simulation temperature, and the stability of their intermediate structures is temperature-dependent. When plotting the stability ranking versus the experimentally determined k_{cat}/K_M values, we observed a logarithmic correlation with an R^2 of 0.82 (Figure 4). When the outlier IMP-1−LOR complex was excluded, R^2 increased to 0.97.

Table 1: Stability of Different Complexes at Different Temperatures[a]

	IMP-1−CEF			IMP-6−CEF			IMP-1−CTX			IMP-6−CTX			IMP-1−LOR			IMP-6−LOR			IMP-1−CAZ			IMP-6−CAZ		
	1[b]	2[b]	3[b]	1[b]	2[b]	3[b]	1[b]	2[b]	3[b]	1[b]	2[b]	3[b]	1[b]	2[b]	3[b]	1[b]	2[b]	3[b]	1[b]	2[b]	3[b]	1[b]	2[b]	3[b]
100 K	+	+	+	+	+	+	+	+	+	+	+	+	+	+	+	+	+	+	−	+	+	−	−	+
α	>	>	>	>	>	>	>	>	>	>	>	>	<	<	>	<	>	<		>	<			<
200 K	+	+	+	+	+	+	+	+	+	+	+	+	−	−	+	+	+	−		−	+			−
300 K	+	+	+	+	+	+	+	−	+	+	+	+			−	+	−				−			
SRS	9			9			8			9			4			6			3			1		
k_{cat}/K_M (s^{-1} μM^{-1})[c]	32.5			39.2			16.1			18.3			8.6			1.25			0.35			0.031		

[a] + means the structure is stable at the temperature indicated at the left, and − means the structure is unstable. α is the Zn2−dummy atom−substrate N angle. > means α > 162°. < means α < 162°. SRS is the stability ranking score. [b] Simulation number. [c] Values from ref *21*.

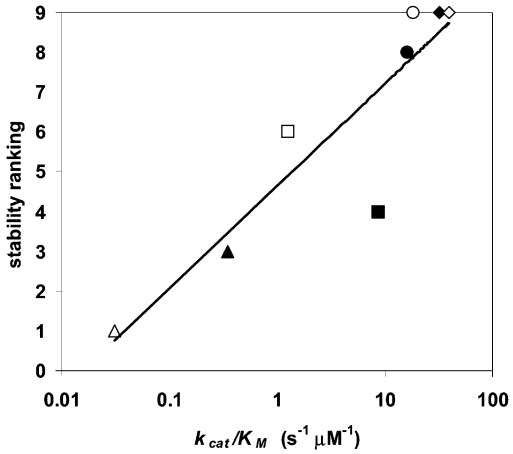

FIGURE 4: Stability rankings obtained with triple simulations plotted vs the k_{cat}/K_M values obtained in experiment on a logarithmic scale: (◆) IMP-1−CEF, (◇) IMP-6−CEF, (●) IMP-1−CTX, (○) IMP-6−CTX, (■) IMP-1−LOR, (□) IMP-6−LOR, (▲) IMP-1−CAZ, and (△) IMP-6−CAZ ($R^2 = 0.82$).

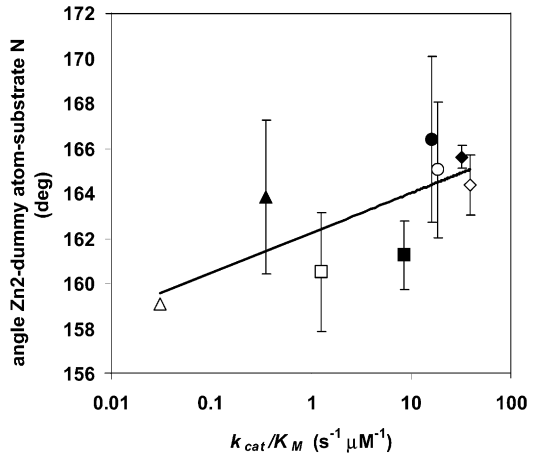

FIGURE 5: Average α (Zn2−dummy atom−substrate nitrogen angle) from triple simulations plotted vs the k_{cat}/K_M values obtained in experiment on a logarithmic scale: (◆) IMP-1−CEF, (◇) IMP-6−CEF, (●) IMP-1−CTX, (○) IMP-6−CTX, (■) IMP-1−LOR, (□) IMP-6−LOR, (▲) IMP-1−CAZ (double simulations), and (△) IMP-6−CAZ (single simulation) ($R^2 = 0.54$).

By performing multiple simulations, we can assess a larger conformational space, thus generating a more realistic, statistically more meaningful model of the enzyme−substrate complex. To test if such a beneficial effect could also be seen in the stability score, ranking was performed on the basis of only one simulation for each enzyme−substrate combination at 100 K, resulting in a stability ranking ranging from 0 to 3 (at most one stable structure at 100, 200, and 300 K). The same trend as before was observed (data not shown), but the correlation coefficient was much smaller ($R^2 = 0.63$).

Molecular Mechanism of Destabilization. To identify the molecular mechanism of how changes in substrate structure and replacement of Ser196 with glycine led to a substrate-specific destabilization, trajectories and average structures of the 100 K simulations were geometrically analyzed. Simulations at 100 K yielded at least one stable complex for all enzyme−substrate combinations (Table 1). Examination of trajectories of unstable complexes showed that the breakdown was always due to the anionic nitrogen of the substrate losing contact with Zn2, as observed for the 300 K simulations of unstable structures (Figures 2 and 3). Before the loss of contact, the angle α between Zn2, the dummy atom, and the nitrogen gradually decreased, whereas the distance between the dummy atom and the substrate nitrogen remained constant until it suddenly increased (data not shown). Thus, the nitrogen was moving out of the zinc coordination sphere tangentially rather than radially. The role of α in predicting stability was supported by analyzing its average value for the stable complexes (Figure 5). A correlation between the measured angles and the experimental k_{cat}/K_M values was observed (Figure 5, $R^2 = 0.54$). Angles between zincs, dummy atoms, and the other zinc ligands (His77, His79, His139, and the substrate carboxylate, coordinating Zn1, and Asp81, Cys158, and His197, coordinating Zn2) were typically close to the ideal, unstrained angle of 180°. In enzyme−substrate complexes that exhibited low enzymatic efficiency, the ideal coordination of the anionic substrate nitrogen to Zn2 was disturbed and α decreased far below 180°, in extreme cases causing the breakdown of the intermediate structure. Visual inspection (Figures 1, 4, and 5) suggests that interaction with R_2 is dominating these effects. Substrates with an acetoxy moiety (CEF and CTX) have a score of 8 or 9 in the stability ranking (Table 1), and their average α is more than 164° (Figure 5). In contrast, the substrates with a positively charged pyridinium moiety at this position only reach scores between 1 and 6 in the stability ranking, and α is less than 164° on average. The interaction of R_2 with four amino acids in the binding site (backbone and side chain of Asn167 and side chains of Lys161, Trp28, and His197) was investigated by measuring distances between the ester oxygen or the corresponding pyridinium nitrogen of the substrate and nitrogen atoms in the four residues. While the distances to Lys161, Trp28, and His197 showed no correlation with k_{cat}/K_M (data not shown), the distances between the Asn167 side chain and backbone nitrogen, and the ester oxygen or the pyridinium nitrogen, clustered. For the substrates with a pyridinium residue (LOR and CAZ), the Asn167 side chain nitrogen−pyridinium

Table 2: Flexibility of His197 Side Chain at Different Temperatures (average rmsd in 10^{-2} Å)[a]

	IMP-1−CEF	IMP-6−CEF	IMP-1−CTX	IMP-6−CTX	IMP-1−LOR	IMP-6−LOR	IMP-1−CAZ	IMP-6−CAZ
100 K	3.10 ± 0.22	3.36 ± 0.29	2.98 ± 0.06	3.46 ± 0.62	3.00 ± 0.03	3.13 ± 0.21	2.98 ± 0.03	2.97
200 K	4.47 ± 0.14	4.46 ± 0.13	4.40 ± 0.21	4.65 ± 0.23	4.40	4.50 ± 0.28	4.34	
300 K	5.74 ± 0.32	7.61 ± 0.03	5.45 ± 0.18	5.55 ± 0.11		5.70		

[a] If no standard deviation is indicated, only one simulation was stable. If no rmsd is indicated, no simulation was stable.

nitrogen distance was 9.3 ± 0.9 Å and the Asn167 backbone nitrogen−pyridinium nitrogen distance was 5.9 ± 0.5 Å. For substrates with an ester residue (CEF and CTX), the distances were significantly shorter: 7.5 ± 1.0 and 4.6 ± 1.2 Å, respectively. In three of 12 average structures with CEF and CTX, the distances between the ester oxygen and the Asn167 backbone nitrogen were 3.0−3.2 Å, indicating hydrogen bonds. Additionally, in eight of these 12 structures, the carbonyl oxygen of the ester group seemed to interact with the side chain nitrogen of Lys161 at a distance of 4.1 ± 0.5 Å. These observations indicate that ester groups are electrostatically held in place by Asn167 and Lys161 or even hydrogen-bonded to Asn167. There are no such interactions with pyridinium moieties. Instead, they are rather repelled toward His197, a ligand of Zn2, although no significant trend in the distances between its side chain and the substrate could be detected.

Effect of the Gly196Ser Mutation on Hydrolysis. We assumed that the Gly196Ser mutation affects the catalytic efficiency via His197, a zinc ligand critical for β-lactam hydrolysis (*43*). This possibility was investigated in two ways. (i) Average structures of the two enzymes with the same substrate at 100 K simulations were superposed using the backbone atoms, and the loop regions comprising residues 192−202 were compared. In the IMP-6 complexes, the side chain of His197 and the backbone of the loop of residues 192−202 were located in slightly different positions compared to the positions in the IMP-1 complexes. However, these differences were too small (generally <1 Å) to significantly alter the geometry of the active site. In regions distant from the active site, the positions of identical atoms deviated by as much as 3 Å in different simulations. (ii) The flexibility of the His197 side chain was measured in terms of the average rmsd with the average structures as a reference for all three simulation temperatures. The rmsd increased with increasing temperatures, and for the IMP-6 complexes, higher rmsd were observed than for the respective IMP-1 complexes with all substrates at all temperatures (Table 2). Exceptions were CEF at 200 K and CAZ at 100 K, where the average rmsd were nearly identical for both proteins. This indicates that for all substrates (except CAZ, for which only few stable complexes were available) the His197 side chain was more flexible in IMP-6 than in IMP-1.

One possible mechanism for the increased flexibility of His197 in IMP-6 is the following. The hydroxyl group of Ser196 interacts with the side chain nitrogen of Lys33. In the crystal structure [PDB entry 1DD6, molecule A (*18*)], the carbonyl oxygen of Pro32, the direct neighbor of Lys33, tightly interacts with Nδ of His197 at a distance of 2.8 Å. In the absence of the Ser196 hydroxyl group, both Lys33 and Pro32 could move. This movement would lead to a decreased stabilization and higher flexibility of His197. This possibility was tested by measuring the distances between the Ser196 hydroxyl oxygen and the Lys33 side chain

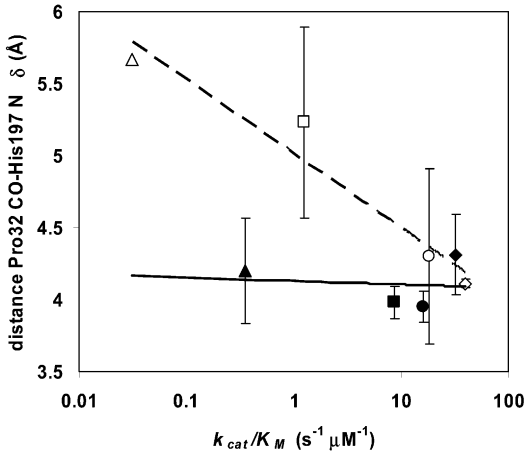

FIGURE 6: Average distances between the Pro32 carbonyl oxygen and His197 Nδ from triple simulations plotted vs the k_{cat}/K_M values obtained in experiment on a logarithmic scale: (◆) IMP-1−CEF, (◇) IMP-6−CEF, (●) IMP-1−CTX, (○) IMP-6−CTX, (■) IMP-1−LOR, (□) IMP-6−LOR, (▲) IMP-1−CAZ (double simulations), and (△) IMP-6−CAZ (single simulation). The solid line is the logarithmic regression trend line of the values with IMP-1 (R^2 = 0.01), and the dashed line is the logarithmic regression trend line of the values with IMP-6 (R^2 = 0.94).

nitrogen and between the Pro32 carbonyl oxygen and His197 Nδ in the average structures after the 100 K simulations. The average of the former distances in all IMP-1 complexes was 4.2 ± 0.8 Å. The latter distances were averaged for each enzyme−substrate complex and plotted versus the k_{cat}/K_M values from experiment (*21*) (Figure 6). In the IMP-1 complexes, the Pro32 carbonyl oxygen−His197 Nδ distance was relatively constant with an average of 4.1 ± 0.2 Å and independent of catalytic efficiency. In contrast, in the IMP-6 complexes, the average distance was longer (4.8 ± 0.7 Å), and it was dependent on catalytic efficiency in a logarithmic manner. Whereas in complexes with mutation-insensitive substrates (CEF and CTX) the distance remained short, it increased in complexes with mutation-sensitive substrates (LOR and CAZ).

DISCUSSION

Ranking of Enzyme−Substrate Intermediate Complexes by Stability. The creation of the ESBL IMP-1 by exchanging a single residue, Gly196 in IMP-6 with serine, is remarkable, since this position is not part of the catalytic machinery, nor is it conserved in the family of metallo-β-lactamases. Even more, it is not in direct contact with the substrate, but at a distance of more than 7 Å. Most interestingly, replacing Gly196 with serine did not lead to an overall increase in activity, but the effect is substrate-specific. Toward two substrates, the cephalosporins CEF and CTX, the mutation is neutral, but toward the two cephalosporins LOR and CAZ as well as for penicillins and the carbapenem imipenem, the mutation leads to a considerable increase in catalytic ef-

ficiency. Modeling of eight enzyme−substrate complexes by unconstrained MD simulations in explicit water indicates that there is no obvious difference in the shape of the binding sites of IMP-6 and IMP-1. Thus, the mutation has a rather subtle effect on the stabilization of the transition state of the substrate. Using multiple MD simulations at different temperatures, the stability of the complexes was evaluated, and a scoring scheme could be established which correlates with the experimentally determined catalytic efficiency. This approach is based on the assumption that k_{cat}/K_M depends on the energy barrier of the rate-limiting step in the hydrolysis of β-lactams. In the enzyme-catalyzed reaction, the barrier of the uncatalyzed reaction is reduced by the binding energy of a substrate in its transition state. As it is difficult to represent the transition state by MD simulation techniques, we chose an intermediate structure just before the rate-limiting step. The logarithmic dependence of the ratio of stable complexes (N_{stable}/N_0) and the catalytic efficiency k_{cat}/K_M can be deduced from the Arrhenius equation (eq 1)

$$k_{cat}/K_M = Ae^{-(U_0-\Delta U)/(RT)} \quad (1)$$

where $U_0 - \Delta U$ is the difference between the activation energy of the uncatalyzed reaction U_0 and the stabilization energy ΔU of the anionic intermediate in complex with the metallo-β-lactamase, A is a reaction-specific constant, R is the universal gas constant, and T is the temperature.

On the other hand, stability ranking is based on a Boltzmann distribution. At a given temperature T, the ratio of stable complexes N_{stable}/N_0 depends on the binding energy ΔU (eq 2).

$$N_{stable}/N_0 = 1 - e^{-\Delta U/(RT)} \quad (2)$$

For small values of N_{stable}/N_0, eqs 1 and 2 can be easily combined, using the approximation $\log(1 - x) \approx -x$ and the constant $c = -\log[Ae^{-U_0/(RT)}]$ (eq 3).

$$c + \log(k_{cat}/K_M) = -\log(1 - N_{stable}/N_0) \approx N_{stable}/N_0 \quad (3)$$

As a consequence, the ratio of stable structures should be proportional to the logarithm of the catalytic efficiency. A high catalytic efficiency corresponds to a high probability that an enzyme−substrate complex remains stable within the 200 ps interval at increasing temperatures, whereas a low catalytic efficiency corresponds to a low probability that the complex remains stable. The instability of the complex is indicated by the breakdown of the enzyme−substrate intermediate complex. This ranking approach does not assume any specific mechanism but is a generic approach to monitoring the relative stability of the intermediate close to the transition state by varying the sequence of the enzyme or the structure of the substrate. Attempts to correlate directly the potential energy of the simulated complexes before the breakdown to experimental data were not successful (data not shown), probably due to energy fluctuations of the ~25000-atom system, in which the interaction of the substrate with the active site plays only a minor role. It should be noted that other procedures for stability ranking may be possible, such as determination of half-life times of the simulated complexes at certain temperatures or gradual heating and determination of the temperature at which the breakdown takes place.

In contrast to determining k_{cat}/K_M by ranking the stability of the substrates in a near-transition state intermediate structure, models of Michaelis complexes of metallo-β-lactamases and still intact β-lactam antibiotics (*17*, *33*−*35*) give insights into the way the substrate binds to the protein prior to hydrolysis, thus estimating K_M. However, little information about catalytic efficiency (k_{cat}/K_M) can be deduced from those complexes, since both k_{cat} and K_M may be modified by a mutation. As an example, the K_M of IMP-1 toward CEF was 5-fold less than the K_M of IMP-6, but k_{cat}/K_M values were almost identical because of a 6-fold decrease in k_{cat} for the IMP-1−CEF complex compared to that for the IMP-6−CEF complex (*21*). In a recent report on substrate binding to the L1 metallo-β-lactamase and different mutants of the enzyme (*44*), it was demonstrated that K_M values were not even reliable for showing substrate binding.

Benefit of Multiple Simulations. A major challenge of MD simulations is adequate sampling of the conformational space (*45*, *46*). As MD trajectories show a sensitive dependence on initial conditions, an ensemble can be efficiently sampled by parallel simulation starting at different initial structures (*46*) or initial velocities (*45*). When multiple 120 ps simulations of crambin were performed with different initial velocities, the overall average structure was closer to the crystal structure than any of the individual trajectory average structures, even when 5 ns trajectories were sampled (*45*). Multiple 5 ns MD simulations of the folding of small peptides (7 and 11 amino acids) with different unfolded initial structures proved to cover a larger conformational space than single 50 ns simulations (*46*). Tens of thousands of 5−20 ns trajectories, starting with different random number seeds in a stochastic dynamics system, were acquired by distributed computing implementation to predict folding of 23-residue proteins from extended structures (*47*). Using a similar approach for the fast-folding 36-residue α-helical protein from the villin headpiece (*48*), the mean of an ensemble of folded structures was found to be more similar to the native fold than any individual folded structure.

When multiple simulations of the different metallo-β-lactamase complexes were performed with different initial velocities, the correlation of the stability ranking with experimental data was more significant than when using only single simulations. On the basis of single simulations, the scores of IMP-1−LOR, IMP-6−LOR, and IMP-1−CAZ complexes were outliers (data not shown) and the correlation of the model and experimental data was low ($R^2 = 0.63$). However, when triple simulations were performed, IMP-6−LOR and IMP-1−CAZ complexes came closer to a logarithmic relationship, resulting in an R^2 of 0.82, while the IMP-1−LOR complex was still an outlier (Figure 4). We assume that if more simulations were carried out, the correlation would continue to be improved. Also, for geometric parameters such as α and the distances measured between R_2 and individual amino acids, better correlations with experimental data were observed with multiple simulations than with single simulations. Although no experimental structures of the modeled systems are available, the improved correlation with kinetic data when performing multiple simulations indicates that, in agreement with the previous reports (*45*, *48*), the average of an ensemble of modeled

structures better describes the actual structure than average structures of individual simulations.

The trends presented herein might be refined by performing more simulations. However, taking into account that each 200 ps simulation took approximately one week of simulation time and generated 600 MB of output, we restricted our investigation to 6-fold simulations at 100 K and triplicate simulations at higher temperatures, which led to a total of 84 simulations.

Interaction of Different Substrates with the Enzymes. Three geometric parameters are related to catalytic efficiency: (i) the angle α between Zn2, the dummy atom oriented toward the substrate nitrogen, and the substrate nitrogen itself, (ii) the distance between R_2 and Asn167 (side chain and backbone nitrogens), and (iii) the distance between the Pro32 carbonyl oxygen and His197 Nδ. In the following, the possible mechanistic relevance of these parameters to substrate specificity is discussed.

The angle α correlated with catalytic efficiency (Figure 5) and with the stability ranking obtained from computational data. Complexes with a small α in the simulations at 100 K were more likely to break down at higher temperatures than complexes with an α close to 180° (Table 1). Four of six structures with an α of <162° at 100 K broke down during the 200 K simulation; one broke down at 300 K, and only one remained stable during the 300 K simulation. In contrast, only one of 15 structures with an α of >162° at 100 K broke down at 200 K and three at 300 K, but 11 were stable at 300 K. The smaller the α, the higher the probability that the nitrogen will be pulled out of its position and replaced with one of the more negatively charged carboxylate oxygens. Whether such a replacement, initiated by a decreased value of α, occurs depends on the stability of the intermediate structure. This again may depend on different factors. (i) The temperature. The higher the simulation temperature was, the fewer stable structures were obtained per complex (Table 1). For the very stable complexes with cephalothin and cefotaxime, most structures remained stable even at 300 K. (ii) The initial velocities. Structures of the same complex could deviate considerably in stability when started with different velocities. In one simulation of the IMP-6−LOR complex, the intermediate structure had already broken down at 100 K (discarded and not included in Table 1), whereas in another simulation, the complex remained stable even at 300 K (Table 1). (iii) The partial charge of the anionic nitrogen of the substrate. The less negatively charged the nitrogen, the higher the likelihood that a more negatively charged atom replaces it. (iv) The structure of the substrate. Complexes with substrates with a pyridinium R_2 group and a more bulky R_1 were less stable than those with an acetoxy R_2 group and a less bulky R_1 (Figures 1 and 4).

The first two factors are systematic, whereas the latter two are substrate-specific. As seen from the report from Iyobe *et al*. (*21*), the investigated cephalosporins can be divided into those with high k_{cat}/K_M values (CEF and CTX) and those with low k_{cat}/K_M values (LOR and CAZ) (Figure 1). The most obvious feature that separates these two pairs is R_2, which is neutral in CEF and CTX (acetoxy) and positively charged in LOR and CAZ (pyridinium). Additionally, the acetoxy group has one more rotatable bond, resulting in a more flexible side chain. This probably affects hydrolysis in two ways. A positively charged pyridinium moiety decreases the negative charge of the anionic nitrogen and therefore makes its replacement more likely. In addition, the positively charged and more rigid pyridinium residue is repelled by Asn167, whereas the acetoxy residue is stabilized by that amino acid. The repulsion of R_2 might assist in dragging the anionic nitrogen out of its ligand position, and as the repulsion is directed toward His197, it might destabilize the coordination of Zn2. The impact of R_2 in MD simulations could be resolved in the stability ranking (Figure 4), the angle α (Figure 5), the geometrical analysis of R_2−Asn167 interactions, and the Pro32−His197 distance in IMP-6 complexes (Figure 6). To the best of our knowledge, a specific interaction of Asn167 with R_2 has not been reported previously. Rather, it was assumed to interact with the β-lactam carbonyl oxygen in the Michaelis complex and the carboxyl group generated by amide bond hydrolysis in the intermediate structure (*5*). We could not observe such an interaction in the IMP-1−CEF complex in MD simulations (*54*), and in experiment, Asn167 [Asn233 according to the standard numbering scheme for class B β-lactamases (*49*)] was not found to be critical for hydrolysis (*50*, *51*).

No significant trends in the distances between R_2 and Lys161, Trp28, and His197 were observed. Lys161 has been shown to be important for hydrolysis of cephalosporins, benzylpenicillin, and imipenem (*50*). Although Lys161 seems to interact with the carbonyl oxygen of the ester group of CEF and CTX, its interaction with the carboxyl moiety at the dihydrothiazine ring of the substrate prevails. Trp28 is located in the flexible loop covering the active site. Deletion of the respective loop in CcrA (*52*) resulted in dramatic losses in hydrolytic activity and affinity for all β-lactams. According to our observations, the interaction of Trp28 with the substrate is not dependent on R_2. As Asn167 pushes R_2 of LOR and CAZ toward His197, a decrease of the distance to that residue was expected but not observed. This might be due to the fact that steric interactions did not allow a further decrease in distance. Indeed, the closest contacts between R_2 and His197 were as small as 2.15 Å for LOR and 2.56 Å for CAZ in average structures at 100 K. The events taking place on the opposite side of His197 relative to R_2, including the interaction of Pro32 and His197, will be the subject of the next section.

R_1 also determines the efficiency of hydrolysis. It is slightly more bulky in CTX than in CEF (k_{cat}/K_M values decreased by ∼50%) and much more bulky in CAZ than in LOR (k_{cat}/K_M values decreased by >95%). The impact of R_1 could be resolved in the stability ranking (Figure 4), but not in α (Figure 5).

Domino Effect of the Gly196Ser Mutation. The Gly196Ser mutation does not have an impact on the hydrolysis of CEF and CTX (acetoxy R_2 group) but does considerably affect hydrolysis of LOR and CAZ (pyridinium R_2 group). We assume that it influences the stability of the substrate intermediate indirectly, most likely via His197. In IMP-1, the His197 side chain is less flexible (Table 2), possibly because of the well-packed region with the serine side chain next to it and because of the stabilization by Pro32 (Figure 6). As a consequence, its coordination to Zn2 could be less sensitive to the substrate R_2 pushing onto it. In contrast, the missing side chain of Gly196 in IMP-6 results in a more flexible His197 side chain which is more sensitive to

repulsive interaction with R_2. The scenario can be interpreted as a "domino effect" involving three dominos: R_2, His197, and the residue at position 196. The side chain of Ser196 is fixed by interaction with surrounding amino acids. When R_2 of the substrates LOR and CAZ pushes toward the His197 side chain, both may lean against the Ser196 side chain and therefore do not fall. Additionally, His197 is stabilized by Pro32. In contrast, in IMP-6, the side chain at position 196 is lacking, His197 is less stabilized by Pro32, and the two dominos will fall. In contrast, CEF and CTX do not push toward His197; thus, there is no difference between Ser196 and Gly196.

Such a domino effect could influence the stability of the intermediate structure in two ways. (i) The coordination of Zn2 could be disturbed, resulting in a less stable intermediate structure. Even Zn2 could be absent. Mutational analysis of IMP-1 showed that His197 is critical for binding of two zinc ions and full enzymatic activity (*43*). The assumption that the second zinc could be absent would be in agreement with the observation that a genetically engineered mononuclear CcrA variant exhibited a catalytic efficiency decreased 10-fold compared to that of the binuclear wild type (*20*). In experiment, the k_{cat}/K_M values of IMP-6−LOR and IMP-6−CAZ complexes were decreased 7- and 10-fold compared to those of IMP-1−LOR and IMP-1−CAZ complexes (*21*). (ii) His197 might simply give way more to R_2, resulting in a more dramatic delocalization of the substrate nitrogen away from its ideal position. Indeed, a significant decrease in α was observed in intermediate structures of enzyme−substrate complexes with low k_{cat}/K_M values (Figure 5), favoring the second possibility. We assume that both effects contribute to the observed results. A similar mechanism seems feasible for IMP, a carbapenem with a positively charged guanidinium group in R_2. This β-lactam is converted poorly compared to cephalothin and cefotaxime and 42 times more efficiently by IMP-1 ($k_{cat}/K_M = 4.2\ s^{-1}\ \mu M^{-1}$) than by IMP-6 ($k_{cat}/K_M = 0.1\ s^{-1}\ \mu M^{-1}$) (*21*). In experiment, the Gly196Ser mutation also had an effect on the hydrolysis of PEN and AMP. The former was hydrolyzed by IMP-1 with a k_{cat}/K_M value of 1.9 $s^{-1}\ \mu M^{-1}$ and by IMP-6 with a value of 0.047 $s^{-1}\ \mu M^{-1}$, the latter with k_{cat}/K_M values of 1.2 and 0.027 $s^{-1}\ \mu M^{-1}$, respectively (*21*). These penicillins do not have a positively charged R_2 but two axial methyl groups at the dihydrothiazole ring, of which one pointed toward His197 in preliminary MD simulations with these β-lactams (data not shown). Thus, it could push onto His197 like the pyridinium moiety.

Our domino effect scenario can be put to the test by comparing it to mutation analyses with IMP-1 (*50*, *51*) and CcrA (*52*, *53*). While IMP-1 has a Ser in position 196 (position 262 according to ref *49*), in CcrA this amino acid is Gly, like in IMP-6. The k_{cat}/K_M values of the wild types in those reports are on the same order of magnitude as those determined for IMP-1 (*21*). When Asn233 (*49*) is mutated to Ala, Asp, and Leu, no significant changes were observed for the hydrolysis of CEF (*50*). For the Asp mutant, the k_{cat}/K_M values for PEN (*50*, *53*) and LOR (*52*, *53*) also remained on the same order of magnitude. With the Ala mutants, PEN was converted even more efficiently [1.8-fold for IMP-1 (*50*) and 1.3-fold for CcrA (*53*)]. Ala has a smaller side chain than Asn and could result in less steric interaction with the axial methyl group in PEN. However, when Asn233 (*47*) was substituted for Leu in CcrA, k_{cat}/K_M values for PEN and LOR were only 15 and 8% of those of wild-type CcrA, respectively (*53*). This can be explained by the more bulky side chain of Leu relative to Asn, Ala, and Asp, interacting sterically with the axial methyl group of PEN and the pyridinium moiety of LOR, thus increasing the pressure of R_2 on Zn2-coordinating His263 (*49*), corresponding to His197 in IMP-1. These experimental data fit in our model.

The discussed mechanisms are consistent with the concept that in IMP-1 Ser196 improves the packing and decreases the flexibility of His197. No hydrogen bonds between the Ser196 hydroxyl group and other residues were observed in our simulations. Thus, it would be interesting to examine if structurally similar residues such as Ala, Val, or Thr could exert the same function as Ser at position 196. Also, investigating if CcrA could obtain a wider substrate spectrum, just like IMP-1, with a Gly → Ser mutation in position 262 (*49*) would be worthwhile. The presented data give a plausible explanation for how IMP-1 has obtained an extended substrate spectrum toward β-lactam antibiotics and, thus, has become a challenge to the treatment of infectious diseases. In general, such mechanisms might play an important role in the evolution of enzymatic activity.

ACKNOWLEDGMENT

We thank Florian Barth, Institute of Technical Biochemistry, University of Stuttgart, for LINUX cluster maintenance and assistance with *Amber 6.0*, and acknowledge the valuable suggestions by the referee regarding the Pro32−His197 interaction.

REFERENCES

1. Laraki, N., Franceschini, N., Rossolini, G. M., Santucci, P., Meunier, C., de Pauw, E., Amicosante, G., Frere, J. M., and Galleni, M. (1999) Biochemical characterization of the *Pseudomonas aeruginosa* 101/1477 metallo-β-lactamase IMP-1 produced by *Escherichia coli*, *Antimicrob. Agents Chemother. 43*, 902−906.
2. Riccio, M. L., Franceschini, N., Boschi, L., Caravelli, B., Cornaglia, G., Fontana, R., Amicosante, G., and Rossolini, G. M. (2000) Characterization of the metallo-β-lactamase determinant of *Acinetobacter baumannii* AC-54/97 reveals the existence of bla(IMP) allelic variants carried by gene cassettes of different phylogeny, *Antimicrob. Agents Chemother. 44*, 1229−1235.
3. Hawkey, P. M., Xiong, J., Ye, H., Li, H., and M'Zali, F. H. (2001) Occurrence of a new metallo-β-lactamase IMP-4 carried on a conjugative plasmid in *Citrobacter youngae* from the People's Republic of China, *FEMS Microbiol. Lett. 194*, 53−57.
4. Ambler, R. P. (1980) The structure of β-lactamases, *Philos. Trans. R. Soc. London, Ser. B 289*, 321−331.
5. Wang, Z., Fast, W., and Benkovic, S. J. (1999) On the mechanism of the metallo-β-lactamase from *Bacteroides fragilis*, *Biochemistry 38*, 10013−10023.
6. Suárez, D., and Merz, K. (2001) Molecular Dynamics Simulations of the Mononuclear Zinc-β-lactamase from *Bacillus cereus*, *J. Am. Chem. Soc. 123*, 3759−3770.
7. Lee, W., McDonough, M. A., Kotra, L., Li, Z. H., Silvaggi, N. R., Takeda, Y., Kelly, J. A., and Mobashery, S. (2001) A 1.2-Å snapshot of the final step of bacterial cell wall biosynthesis, *Proc. Natl. Acad. Sci. U.S.A. 98*, 1427−1431.
8. Green, D. W. (2002) The bacterial cell wall as a source of antibacterial targets, *Expert Opin. Ther. Targets 6*, 1−19.
9. Graefe, U. (1992) *Biochemie der Antibiotika, Struktur, Biosynthese, Wirkungsmechanismus*, Spektrum Akademischer Verlag, Heidelberg, Germany.
10. Petrosino, J., Cantu, C., III, and Palzkill, T. (1998) β-Lactamases: protein evolution in real time, *Trends Microbiol. 6*, 323−327.

11. Matagne, A., Lamotte-Brasseur, J., and Frere, J. M. (1998) Catalytic properties of class A β-lactamases: efficiency and diversity, *Biochem. J. 330*, 581−598.
12. Sabath, L. D., and Abraham, E. P. (1966) Zinc as a cofactor for cephalosporinase from *Bacillus cereus* 569, *Biochem. J. 98*, 11C−13C.
13. Payne, D. J. (1993) Metallo-β-lactamases: a new therapeutic challenge, *J. Med. Microbiol. 39*, 93−99.
14. Carfi, A., Pares, S., Duee, E., Galleni, M., Duez, C., Frere, J. M., and Dideberg, O. (1995) The 3-D structure of a zinc metallo-β-lactamase from *Bacillus cereus* reveals a new type of protein fold, *EMBO J. 14*, 4914−4921.
15. Aravind, L. (1999) An evolutionary classification of the metallo-β-lactamase fold proteins, *In Silico Biol. 1*, 69−91.
16. Concha, N. O., Rasmussen, B. A., Bush, K., and Herzberg, O. (1996) Crystal structure of the wide-spectrum binuclear zinc β-lactamase from *Bacteroides fragilis*, *Structure 4*, 823−836.
17. Ullah, J. H., Walsh, T. R., Taylor, I. A., Emery, D. C., Verma, C. S., Gamblin, S. J., and Spencer, J. (1998) The crystal structure of the L1 metallo-β-lactamase from *Stenotrophomonas maltophilia* at 1.7 Å resolution, *J. Mol. Biol. 284*, 125−136.
18. Concha, N. O., Janson, C. A., Rowling, P., Pearson, S., Cheever, C. A., Clarke, B. P., Lewis, C., Galleni, M., Frere, J. M., Payne, D. J., Bateson, J. H., and Abdel-Meguid, S. S. (2000) Crystal structure of the IMP-1 metallo β-lactamase from *Pseudomonas aeruginosa* and its complex with a mercaptocarboxylate inhibitor: binding determinants of a potent, broad-spectrum inhibitor, *Biochemistry 39*, 4288−4298.
19. Fabiane, S. M., Sohi, M. K., Wan, T., Payne, D. J., Bateson, J. H., Mitchell, T., and Sutton, B. J. (1998) Crystal structure of the zinc-dependent β-lactamase from *Bacillus cereus* at 1.9 Å resolution: binuclear active site with features of a mononuclear enzyme, *Biochemistry 37*, 12404−12411.
20. Fast, W., Wang, Z., and Benkovic, S. J. (2001) Familial mutations and zinc stoichiometry determine the rate-limiting step of nitrocefin hydrolysis by metallo-β-lactamase from *Bacteroides fragilis*, *Biochemistry 40*, 1640−1650.
21. Iyobe, S., Kusadokoro, H., Ozaki, J., Matsumura, N., Minami, S., Haruta, S., Sawai, T., and O'Hara, K. (2000) Amino acid substitutions in a variant of IMP-1 metallo-β-lactamase, *Antimicrob. Agents Chemother. 44*, 2023−2027.
22. Watanabe, M., Iyobe, S., Inoue, M., and Mitsuhashi, S. (1991) Transferable imipenem resistance in *Pseudomonas aeruginosa*, *Antimicrob. Agents Chemother. 35*, 147−151.
23. Chu, Y. W., Afzal-Shah, M., Houang, E. T., Palepou, M. I., Lyon, D. J., Woodford, N., and Livermore, D. M. (2001) IMP-4, a novel metallo-β-lactamase from nosocomial *Acinetobacter spp*. collected in Hong Kong between 1994 and 1998, *Antimicrob. Agents Chemother. 45*, 710−714.
24. Da Silva, G. J., Correia, M., Vital, C., Ribeiro, G., Sousa, J. C., Leitao, R., Peixe, L., and Duarte, A. (2002) Molecular characterization of bla(IMP-5), a new integron-borne metallo-β-lactamase gene from an *Acinetobacter baumannii* nosocomial isolate in Portugal, *FEMS Microbiol. Lett. 215*, 33−39.
25. Yano, H., Kuga, A., Okamoto, R., Kitasato, H., Kobayashi, T., and Inoue, M. (2001) Plasmid-encoded metallo-β-lactamase (IMP-6) conferring resistance to carbapenems, especially meropenem, *Antimicrob. Agents Chemother. 45*, 1343−1348.
26. Yan, J. J., Ko, W. C., Tsai, S. H., Wu, H. M., and Wu, J. J. (2001) Outbreak of infection with multidrug-resistant *Klebsiella pneumoniae* carrying bla(IMP-8) in a university medical center in Taiwan, *J. Clin. Microbiol. 39*, 4433−4439.
27. Gibb, A. P., Tribuddharat, C., Moore, R. A., Louie, T. J., Krulicki, W., Livermore, D. M., Palepou, M. F., and Woodford, N. (2002) Nosocomial outbreak of carbapenem-resistant *Pseudomonas aeruginosa* with a new bla(IMP) allele, bla(IMP-7), *Antimicrob. Agents Chemother. 46*, 255−258.
28. Iyobe, S., Kusadokoro, H., Takahashi, A., Yomoda, S., Okubo, T., Nakamura, A., and O'Hara, K. (2002) Detection of a variant metallo-β-lactamase, IMP-10, from two unrelated strains of *Pseudomonas aeruginosa* and an alcaligenes xylosoxidans strain, *Antimicrob. Agents Chemother. 46*, 2014−2016.
29. Helfand, M. S., Hujer, A. M., Sonnichsen, F. D., and Bonomo, R. A. (2002) Unexpected advanced generation cephalosporinase activity of the Met69Phe variant of SHV β-lactamase, *J. Biol. Chem. 277*, 44719−44723.
30. Suarez, D., Brothers, E. N., and Merz, K. M., Jr. (2002) Insights into the Structure and Dynamics of the Dinuclear Zinc β-Lactamase Site from *Bacteroides fragilis*, *Biochemistry 41*, 6615−6630.
31. Pang, Y. P., Xu, K., Yazal, J. E., and Prendergast, F. G. (2000) Successful molecular dynamics simulation of the zinc-bound farnesyltransferase using the cationic dummy atom approach, *Protein Sci. 9*, 1857−1865.
32. Pang, Y. P. (2001) Successful Molecular Dynamics Simulation of Two Zinc Complexes Bridged by a Hydroxide in Phosphotriesterase Using the Cationic Dummy Atom Method, *Proteins 45*, 183−189.
33. Díaz, N., Suárez, D., and Merz, K. (2001) Molecular Dynamics Simulations of the Mononuclear Zinc-β-lactamase from *Bacillus cereus* Complexed with Benzylpenicillin and a Quantum Chemical Study of the Reaction Mechanism, *J. Am. Chem. Soc. 123*, 9867−9879.
34. Toney, J. H., Hammond, G. G., Fitzgerald, P. M., Sharma, N., Balkovec, J. M., Rouen, G. P., Olson, S. H., Hammond, M. L., Greenlee, M. L., and Gao, Y. D. (2001) Succinic acids as potent inhibitors of plasmid-borne IMP-1 metallo-β-lactamase, *J. Biol. Chem. 276*, 31913−31918.
35. Suarez, D., Diaz, N., and Merz, K. M., Jr. (2002) Molecular dynamics simulations of the dinuclear zinc-β-lactamase from *Bacteroides fragilis* complexed with imipenem, *J. Comput. Chem. 23*, 1587−1600.
36. Case, D. A., Pearlman, D. A., Caldwell, J. W., Cheatham, T. E., III, Ross, W. S., Simmerling, C. L., Darden, T. A., Merz, K. M., Jr., Stanton, R. V., Cheng, A. L., Vincent, J. J., Crowley, M., Tsui, V., Radmer, R. J., Duan, Y., Pitera, J., and Massove, I. (1999) *AMBER*, version 6.0, University of California, San Francisco.
37. Yazal, J., and Pang, Y. (1999) Ab Initio Calculations of Proton Dissociation Energies of Zinc Ligands: Hypothesis of Imidazolate as Zinc Ligand in Proteins, *J. Phys. Chem. B 103*, 8773−8779.
38. Huang, C., Lesburg, C. A., Kiefer, L. L., Fierke, C. A., and Christianson, D. W. (1996) Reversal of the Hydrogen Bond to Zinc Ligand Histidine-119 Dramatically Diminishes Catalysis and Enhances Metal Equilibration Kinetics in Carbonic Anhydrase II, *Biochemistry 35*, 3439−3446.
39. Tainer, J. A., Getzoff, E. D., Beem, K. M., Richardson, J. S., and Richardson, D. C. (1982) Determination and analysis of the 2 Å structure of copper, zinc superoxide dismutase, *J. Mol. Biol. 160*, 181−217.
40. Cornell, W. D., Cieplak, P., Bayly, C. I., Gould, I. R., Merz, K. M., Ferguson, D. M., Spellmeyer, D. C., Fox, T., Caldwell, J. W., and Kollman, P. A. (1995) A 2nd Generation Force-Field for the Simulation of Proteins, Nucleic-Acids, and Organic-Molecules, *J. Am. Chem. Soc. 117*, 5179−5197.
41. van Gunsteren, W. F., and Berendsen, H. J. C. (1977) Algorithms for macromolecular dynamics and constraint dynamics, *Mol. Phys. 34*, 1311−1327.
42. Humphrey, W., Dalke, A., and Schulten, K. (1996) VMD: Visual Molecular Dynamics, *J. Mol. Graphics 14*, 33−38.
43. Haruta, S., Yamaguchi, H., Yamamoto, E. T., Eriguchi, Y., Nukaga, M., O'Hara, K., and Sawai, T. (2000) Functional analysis of the active site of a metallo-β-lactamase proliferating in Japan, *Antimicrob. Agents Chemother. 44*, 2304−2309.
44. Carenbauer, A. L., Garrity, J. D., Periyannan, G., Yates, R. B., and Crowder, M. W. (2002) Probing substrate binding to Metallo-β-Lactamase LI from *Stenotrophomonas maltophilia* by using site-directed mutagenesis, *BMC Biochem. 3*, 4.
45. Caves, L. S., Evanseck, J. D., and Karplus, M. (1998) Locally accessible conformations of proteins: multiple molecular dynamics simulations of crambin, *Protein Sci. 7*, 649−666.
46. Smith, L. J., Daura, X., and van Gunsteren, W. F. (2002) Assessing equilibration and convergence in biomolecular simulations, *Proteins 48*, 487−496.
47. Snow, C., Nguyen, H., Pande, V., and Gruebele, M. (2002) Absolute comparison of simulated and experimental protein-folding dynamics, *Nature 420*, 102−106.
48. Zagrovic, B., Snow, C. D., Shirts, M. R., and Pande, V. S. (2002) Simulation of Folding of a Small α-helical Protein in Atomistic Detail using Worldwide-distributed Computing, *J. Mol. Biol. 323*, 927−937.
49. Galleni, M., Lamotte-Brasseur, J., Rossolini, G. M., Spencer, J., Dideberg, O., and Frere, J. M. (2001) Standard numbering scheme

for class B β-lactamases, *Antimicrob. Agents Chemother. 45*, 660−663.
50. Haruta, S., Yamamoto, E. T., Eriguchi, Y., and Sawai, T. (2001) Characterization of the active-site residues asparagine 167 and lysine 161 of the IMP-1 metallo β-lactamase, *FEMS Microbiol. Lett. 197*, 85−89.
51. Materon, I. C., and Palzkill, T. (2001) Identification of residues critical for metallo-β-lactamase function by codon randomization and selection, *Protein Sci. 10*, 2556−2565.
52. Yang, Y., Keeney, D., Tang, X., Canfield, N., and Rasmussen, B. A. (1999) Kinetic properties and metal content of the metallo-β-lactamase CcrA harboring selective amino acid substitutions, *J. Biol. Chem. 274*, 15706−15711.
53. Yanchak, M. P., Taylor, R. A., and Crowder, M. W. (2000) Mutational analysis of metallo-β-lactamase CcrA from *Bacteroides fragilis*, *Biochemistry 39*, 11330−11339.
54. Oelschlaeger, P., Schmid, R. D., and Pleiss, J. (2003) Insight into the mechanism of the IMP-1 metallo-β-lactamase by molecular dynamics simulations, *Protein Eng. 16*, 341−350.

BI0300332